Peropsin modulates transit of vitamin A from retina to retinal pigment epithelium

Jeremy D. Cook[‡], Sze Yin Ng[‡], Marcia Lloyd[‡], Shannan Eddington[‡], Hui Sun[‡§], Jeremy Nathans[¶‖], Dean Bok[‡1], Roxana A. Radu[‡], and Gabriel H. Travis[‡**2]

From the [‡]Department of Ophthalmology, Stein Eye Institute, [§]Department of Physiology, and [**]Department of Biological Chemistry, School of Medicine, UCLA, Los Angeles, California 90095, [¶]Department of Molecular Biology and Genetics, Neuroscience, and Ophthalmology, The Johns Hopkins University School of Medicine, Baltimore, Maryland 21205, and [‖]Howard Hughes Medical Institute, Baltimore, Maryland 21205

Edited by Velia M. Fowler

Peropsin is a non-visual opsin in both vertebrate and invertebrate species. In mammals, peropsin is present in the apical microvilli of retinal pigment epithelial (RPE) cells. These structures interdigitate with the outer segments of rod and cone photoreceptor cells. RPE cells play critical roles in the maintenance of photoreceptors, including the recycling of visual chromophore for the opsin visual pigments. Here, we sought to identify the function of peropsin in the mouse eye. To this end, we generated mice with a null mutation in the peropsin gene (*Rrh*). These mice exhibited normal retinal histology, normal morphology of outer segments and RPE cells, and no evidence of photoreceptor degeneration. Biochemically, *Rrh*$^{-/-}$ mice had ~2-fold higher vitamin A (all-*trans*-retinol (all-*trans*-ROL)) in the neural retina following a photobleach and 5-fold lower retinyl esters in the RPE. This phenotype was similar to those reported in mice that lack interphotoreceptor retinoid-binding protein (IRBP) or cellular retinol-binding protein, suggesting that peropsin plays a role in the movement of all-*trans*-ROL from photoreceptors to the RPE. We compared the phenotypes in mice lacking both peropsin and IRBP with those of mice lacking peropsin or IRBP alone and found that the retinoid phenotype was similarly severe in each of these knock-out mice. We conclude that peropsin controls all-*trans*-ROL movement from the retina to the RPE or may regulate all-*trans*-ROL storage within the RPE. We propose that peropsin affects light-dependent regulation of all-*trans*-ROL uptake from photoreceptors into RPE cells through an as yet undefined mechanism.

The opsins are members of the G protein–coupled receptor superfamily. Visual perception begins with the absorption of a photon by an opsin pigment in a rod or cone photoreceptor cell. The light-absorbing chromophore in most visual opsins is 11-*cis*-retinaldehyde (11-*cis*-RAL),[3] which is covalently coupled to the protein through a Schiff-base linkage. Absorption of a photon isomerizes the ligand to all-*trans*-RAL, activating the pigment. After a brief signaling period, the activated metarhodopsin II/III decays by releasing all-*trans*-RAL into the outer segment (OS) disk membrane. Restoration of light sensitivity to the resultant apo-opsin occurs after it recombines with another 11-*cis*-RAL. The conversion of all-*trans*-RAL back to 11-*cis*-RAL is carried out by multistep enzyme pathways in the retinal pigment epithelium (RPE) (1) and Müller cells of the retina (2–4). Non-enzymatic photoisomerization of retinyl lipids also contributes to 11-*cis*-RAL synthesis and visual pigment regeneration (5). Rhodopsin and the cone-opsin visual pigments are considered *bleaching* opsins because the retinaldehyde ligand dissociates after photoisomerization.

Besides the visual pigments, the mammalian retina also contains several non-visual opsins. These pigments are more closely related to the rhabdomeric photoreceptor opsins of invertebrates than to the vertebrate visual opsins. The best characterized non-visual opsin is melanopsin (Opn4), which is present in a subset of retinal ganglion neurons and mediates circadian photoentrainment (6, 7) and part of the pupillary light response (8). Another non-visual opsin is "retinal G protein–coupled receptor" (RGR) opsin, which is expressed in the internal membranes of RPE and Müller glial cells (9). RGR opsin may function as a photoisomerase that regenerates visual chromophore based on the phenotype of mice that lack RGR opsin (10) and its similarity to the known photoisomerase squid retinochrome (11). RGR opsin was also shown to affect light-dependent mobilization of all-*trans*-retinyl esters (all-*trans*-REs) in mouse RPE cells (12). Neuropsin (OPN5) is a UV-sensitive bistable pigment also expressed in the vertebrate retina (13, 14) that may play an additional role in photoentrainment (15, 16).

The fourth non-visual opsin in the vertebrate retina is "RPE-derived rhodopsin homologue" (RRH), also called peropsin.

[3] The abbreviations used are: RAL, retinaldehyde; RPE, retinal pigment epithelium; OS, outer segment(s); ROL, retinol; IRBP, interphotoreceptor retinoid-binding protein; CRBP1, cellular retinol-binding protein 1; RGR, retinal G protein–coupled receptor; RE, retinyl ester; RRH, RPE-derived rhodopsin homologue; LRAT, lecithin–retinol acyltransferase; RAc, retinyl acetate; IPM, interphotoreceptor matrix.
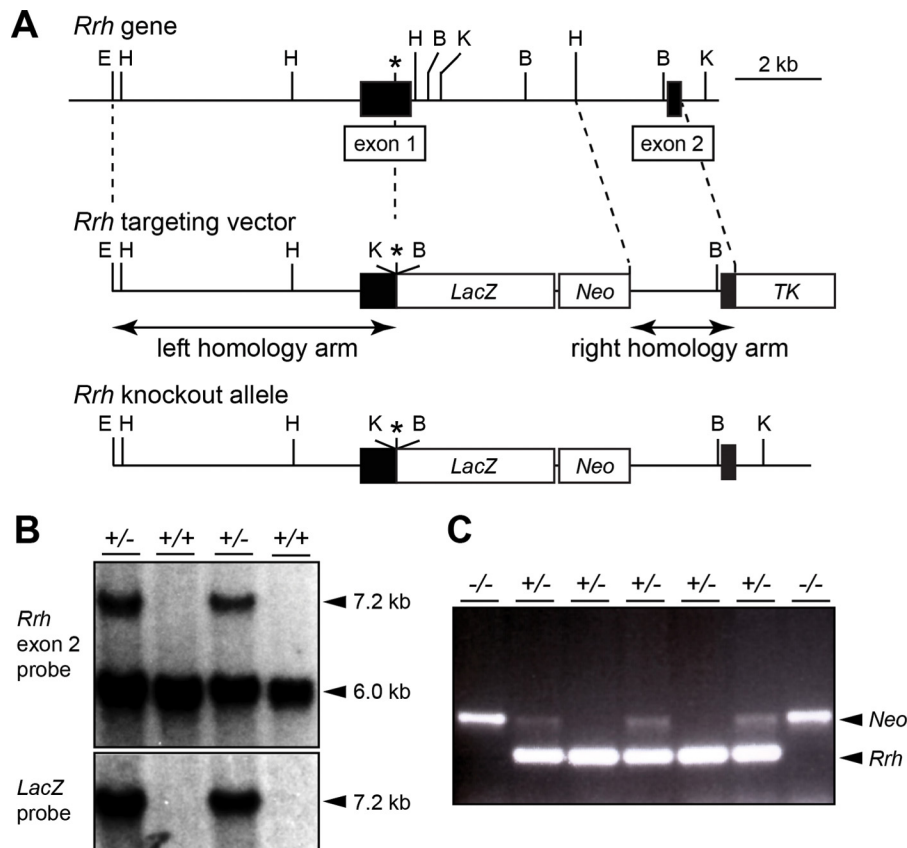
Figure 1. Gene targeting of the murine *Rrh* gene. *A*, restriction maps of the mouse *Rrh* gene (*top*), the targeting construct (*middle*), and the predicted structure of the targeted gene (*bottom*). The first and second *Rrh* exons are shown as *filled boxes*. *Neo*, the *PGK-Neo* cassette; *TK*, the *MC1-TK* cassette; *LacZ*, the *E. coli LacZ* gene; *E*, EcoRI; *H*, HindIII; *B*, BamHI; *K*, KpnI. The *asterisk* indicates the *Rrh* initiator methionine codon. *B*, screening of heterozygous and homozygous mutants of the *Rrh* gene. Shown is Southern blot analysis of KpnI-digested tail DNA isolated from progeny of a chimeric mouse. The blot on the *top* was probed with a DNA segment derived from *Rrh* exon 2. The blot on the *bottom* was probed with a *LacZ* probe. *C*, PCR analysis of tail DNA. The *upper* PCR product detects the presence of the *Neo* cassette. The *lower* PCR product detects the presence of the *Rrh* gene, which is eliminated in a homozygous knock-out. +/+, wild type; +/− heterozygous mutant; −/− homozygous mutant.

Currently, very little is known about this protein despite it having been discovered 20 years ago (17). Mammalian peropsin is 28% identical to rhodopsin and 31% identical to melanopsin. Chromophore regeneration studies of peropsin homologues suggest that it binds all-*trans*-RAL in the dark and converts it to 11-*cis*-RAL upon exposure to visible light (18, 19) akin to RGR opsin (20). Similar to the other non-visual opsins, peropsin is likely a *bistable* opsin whereby the retinaldehyde chromophore remains coupled to the protein after photoisomerization (21). Peropsin is located exclusively in the apical microvilli of RPE cells (17). These cellular processes interdigitate closely with the OS of rods and cones. The RPE performs several functions critical to the maintenance of photoreceptor viability and light sensitivity (22). Besides hosting the visual cycle for chromophore regeneration, RPE cells provide nutrition to photoreceptors, maintain fluid and electrolyte balance in the retina, and diurnally phagocytose the shed tips of distal rod and cone OS (23, 24). A recent report also suggests peropsin expressed in skin confers photosensitivity to short-wavelength light (25).

In the current study, we set out to define the function of a mammalian peropsin. To this end, we generated mice with a null mutation in the gene for peropsin and studied the resulting ocular phenotype. In particular, we examined retinal morphol-ogy in $Rrh^{-/-}$ mice by light and electron microscopy. We also determined the content of visual retinoids in eye tissues from wild-type and $Rrh^{-/-}$ mice under different light conditions. Finally, we measured protein levels and catalytic activities of visual cycle proteins. The results of these studies indicate that peropsin (i) modulates movement of vitamin A from the retina to the RPE and/or (ii) modulates storage of vitamin A within the RPE.

Results

Generation of mice that lack peropsin

As a first step toward understanding the function of peropsin, we generated $Rrh^{-/-}$ mice by homologous recombination in embryonic stem cells. The knock-out construct is shown in Fig. 1*A*, and confirmation of homologous recombination by Southern blotting is shown in Fig. 1*B*. Genotyping of offspring by PCR analysis is shown in Fig. 1*C*. To confirm abrogation of peropsin expression, we performed immunoblot analysis on RPE homogenates from wild-type and $Rrh^{-/-}$ homozygous mice. As expected, the band corresponding to the 37-kDa peropsin protein is absent in lanes containing $Rrh^{-/-}$ homogenates (Fig. 2*A*). Immunohistochemistry of eyecup sections showed an immunofluorescent signal with antiserum to perop-
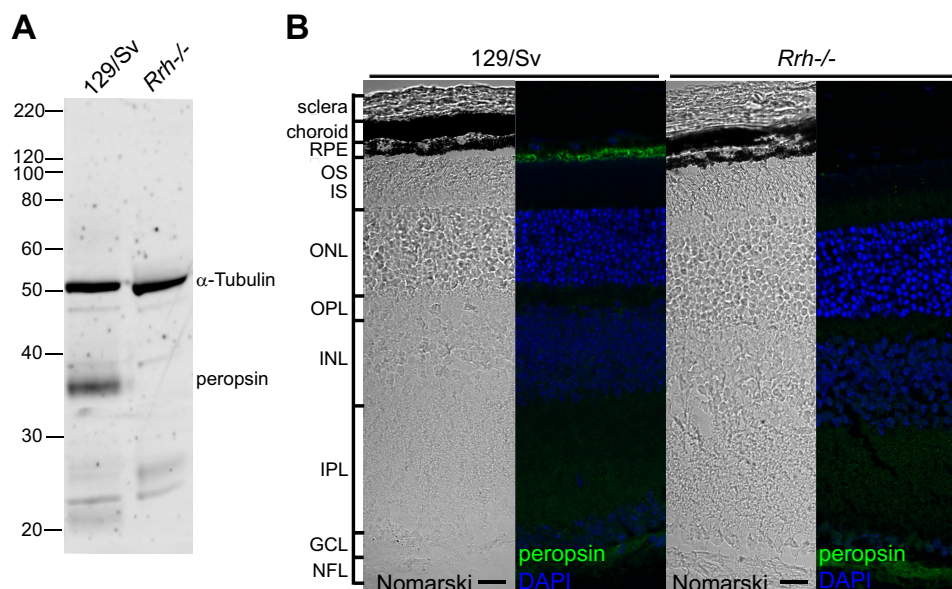
Figure 2. Peropsin (RRH) expression in the RPE. *A*, Western blot analysis of 129/Sv and $Rrh^{-/-}$ mouse eyecup homogenates. Peropsin migrates as a 37-kDa band and is not present in RPE collected from the $Rrh^{-/-}$ mice. *B*, immunohistochemical analysis of peropsin (*green*) expression in RPE of mouse eyecups. Nuclei were counterstained with DAPI (*blue*). Labels identifying the retinal layers are shown to the *left* of the Nomarski image. *NFL*, nerve fiber layer; *GCL*, ganglion cell layer; *IPL*, inner plexiform layer; *INL*, inner nuclear layer; *OPL*, outer plexiform layer; *ONL*, outer nuclear layer; *IS*, photoreceptor inner segments. Images are representative of at least three independent experiments. *Scale bars*, 20 μm.

sin in the RPE of wild-type sections that was absent in sections from $Rrh^{-/-}$ mice (Fig. 2*B*). Besides the RPE, no other cells exhibited peropsin immunofluorescence.

Retinas of $Rrh^{-/-}$ mice have normal morphology

Photoreceptors are critically dependent on RPE cells for viability. To test whether the absence of peropsin causes photoreceptor degeneration, we examined $Rrh^{-/-}$ retina sections by light microscopy. $Rrh^{-/-}$ retinas were indistinguishable from wild type (Fig. 3, *A* and *B*). Quantification of retinal thickness across the entire eye revealed no loss of photoreceptor nuclei in the outer nuclear layer (Fig. 3*E*). Electron microscopy of outer retina sections from $Rrh^{-/-}$ mice revealed qualitatively normal RPE (Fig. 4, *A* and *B*) with normal basal infoldings (Fig. 4, *A'* and *B'*) and apical microvilli (Fig. 4, *A''* and *B''*). Similarly, the photoreceptor OS appeared normal with regular and well aligned disks (Fig. 4, *A''* and *B''*). No debris was present in the subretinal space between the OS and RPE. Loss of peropsin therefore did not affect distal retinal histology or the ultrastructure of photoreceptor OS and RPE cells.

Retinoid dynamics in $Rrh^{-/-}$ mice

A possible function of peropsin is light-dependent regulation of the visual cycle in RPE cells through interaction with G_q or another G protein. Alternatively, because peropsin binds all-*trans*-RAL in the dark and converts it to 11-*cis*-RAL upon light exposure (18), peropsin may function as a photoisomerase for synthesis of chromophore to regenerate visual pigments.

To test these possible functions of peropsin, we measured levels of visual retinoids in neural retinas and RPE from 1-month-old wild-type (129/Sv) and $Rrh^{-/-}$ mice exposed to different light conditions. Retinoids were examined in mice after overnight dark adaptation, immediately following light

exposure, and at different times during recovery in darkness as described previously (26). Wild-type and $Rrh^{-/-}$ mice exposed to a 1,000-lux light for 5 min exhibited 2-fold reductions in levels of 11-*cis*-RAL (Fig. 5*A*), indicating ~50% photobleach of rhodopsin in mice of both genotypes (p values <0.001). Levels of 11-*cis*-RAL were similar in wild-type and $Rrh^{-/-}$ retinas under all tested conditions (p values >0.122) (Fig. 5*A*). These results suggest that peropsin plays no significant role in the synthesis of visual chromophore.

Two notable differences emerged between wild-type and $Rrh^{-/-}$ mice in the retinoid dynamics study. First, levels of all-*trans*-ROL were 2-fold higher in $Rrh^{-/-}$ retinas at 5 min after the photobleach ($p = 0.003$) with reversion toward normal during recovery (Fig. 5*B*). Second, all-*trans*-REs were 5-fold lower in dark-adapted $Rrh^{-/-}$ RPE ($p < 0.001$) (Fig. 5*C*). Retinyl esters normally increase in the RPE after a photobleach due to uptake and esterification of all-*trans*-ROL released by the photoreceptors. Retinyl esters increased in $Rrh^{-/-}$ RPE after light exposure but more slowly than in wild-type RPE (Fig. 5*C*). After 45 min of postbleach recovery, all-*trans*-RE levels were similar in mice of the two genotypes. Besides these changes, levels of visual retinoids were similar between wild-type and $Rrh^{-/-}$ retinas and RPE under the various light conditions.

Retinyl esters normally build up in mouse RPE during the first few months of postnatal life (27). To test whether this occurs in RPE without peropsin, we measured all-*trans*-RE in eyes from dark-adapted wild-type and $Rrh^{-/-}$ mice at 1 through 4 months of age. Although all-*trans*-RE increased 4-fold in wild-type mice, we observed only a slight increase in all-*trans*-RE in $Rrh^{-/-}$ RPE during the same period ($p < 0.001$) (Fig. 5*D*). The failure of $Rrh^{-/-}$ mice to build their stores of all-*trans*-REs with age indicates that loss of peropsin has a long-term impact on vitamin A metabolism in the RPE.

A **B** **C** **D**
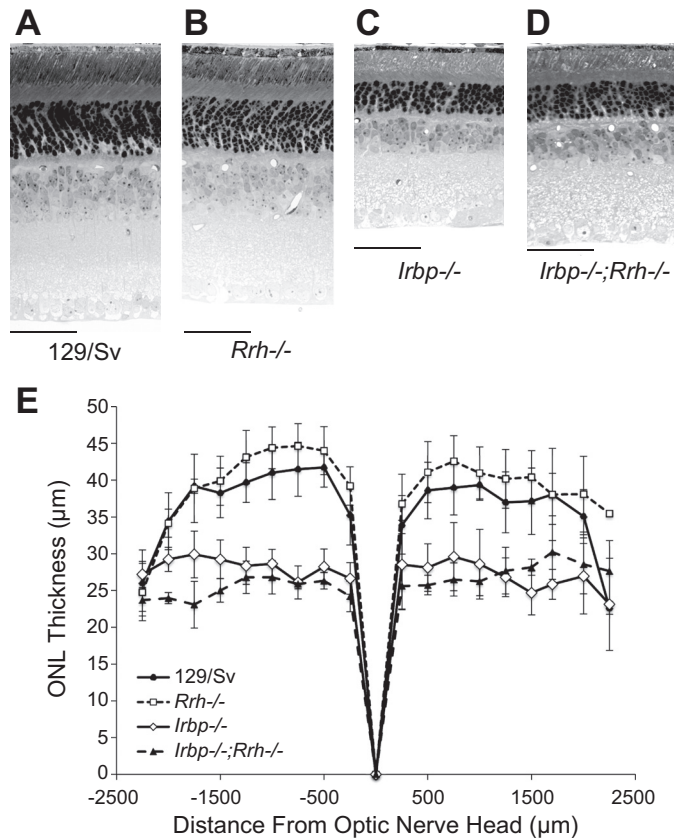
Irbp-/- *Irbp-/-;Rrh-/-*

129/Sv *Rrh-/-*

E

Figure 3. Retinal thickness measurements of 129/Sv, *Rrh*$^{-/-}$, *Irbp*$^{-/-}$, and *Irbp*$^{-/-}$;*Rrh*$^{-/-}$ mice. *A–D*, light microscope images of representative fixed sections from 1-month-old 129/Sv (*A*), *Rrh*$^{-/-}$ (*B*), *Irbp*$^{-/-}$ (*C*), and *Irbp*$^{-/-}$;*Rrh*$^{-/-}$ (*D*) mouse retinas. Sections are from ~1 mm below the optic nerve head. Retinas from 1-month-old *Rrh*$^{-/-}$ mice show no signs of photoreceptor degeneration, whereas retinas from *Irbp*$^{-/-}$ and *Irbp*$^{-/-}$;*Rrh*$^{-/-}$ mice of the same age show ~50% degeneration. *Scale bars*, 50 μm. *E*, spidergram quantifying outer nuclear layer (*ONL*) thicknesses for all genotypes across the entire retina. Images and quantification are representative of *n* = 3 mice; *error bars* represent S.D. *Rrh*$^{-/-}$ retinas were thicker than 129/Sv (*p* = 0.018), and *Irbp*$^{-/-}$ and *Irbp*$^{-/-}$;*Rrh*$^{-/-}$ retinas were significantly thinner than 129/Sv (*p* values <0.001).

Studies on mice lacking both peropsin and IRBP

The phenotypic pattern of elevated all-*trans*-ROL in the retina and reduced all-*trans*-RE in the RPE (Fig. 5, *B* and *C*) was previously observed in *Irbp*$^{-/-}$ mice that lack IRBP (26, 28). IRBP binds all-*trans*-ROL and 11-*cis*-RAL during transit through the extracellular space between photoreceptor OS and the apical RPE. Transit of all-*trans*-ROL from the retina to the RPE is delayed but not blocked in mice lacking IRBP or peropsin, implying the existence of redundant transit pathways. If IRBP and peropsin were components of separate pathways, we would predict a more severe retinoid phenotype in mice lacking both IRBP and peropsin. To test this possibility, we generated mice with null mutations in both the *Irbp* and *Rrh* genes. We repeated the retinoid dynamics experiment on *Irbp*$^{-/-}$ and *Irbp*$^{-/-}$;*Rrh*$^{-/-}$ mice. Similar to *Rrh*$^{-/-}$ mice, levels of all-*trans*-ROL were elevated in *Irbp*$^{-/-}$ (*p* = 0.019) and *Irbp*$^{-/-}$; *Rrh*$^{-/-}$ retinas (*p* < 0.001) relative to wild-type retinas following exposure to light (Fig. 5*B*). Furthermore, in a dark-adapted state, the levels of all-*trans*-RE in *Irbp*$^{-/-}$ and *Irbp*$^{-/-}$;*Rrh*$^{-/-}$ RPE were comparable with that in *Rrh*$^{-/-}$ (Fig. 5*C*). Therefore, loss of both peropsin and IRBP caused similar slowing of all-
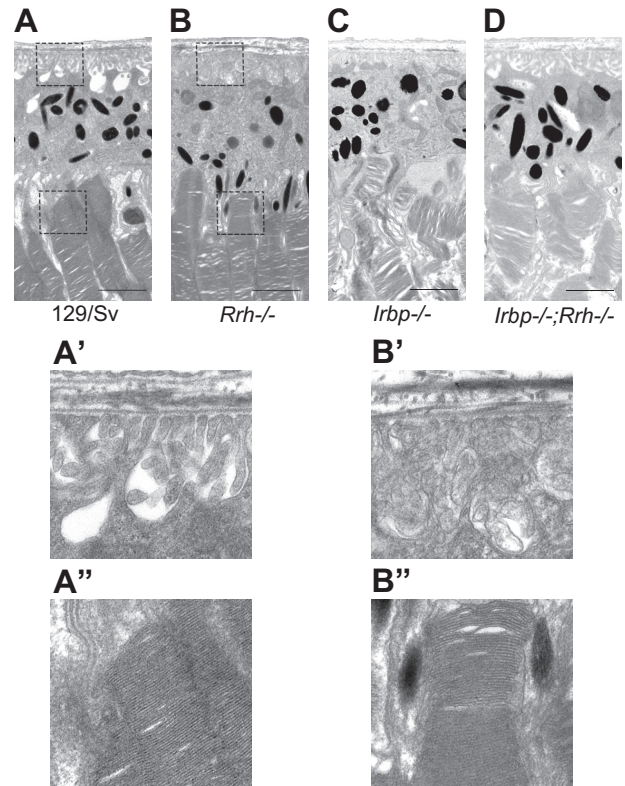

A **B** **C** **D**

129/Sv *Rrh-/-* *Irbp-/-* *Irbp-/-;Rrh-/-*

A' **B'**

A" **B"**

Figure 4. Ultrastructure of RPE and distal photoreceptor OS in sections from 129/Sv, *Rrh*$^{-/-}$, *Irbp*$^{-/-}$, and *Irbp*$^{-/-}$;*Rrh*$^{-/-}$ mice. *A–D*, electron microscope images of plastic-embedded tissue sections from 1-month-old 129/Sv (*A*), *Rrh*$^{-/-}$ (*B*), *Irbp*$^{-/-}$ (*C*), and *Irbp*$^{-/-}$;*Rrh*$^{-/-}$ (*D*) mouse retinas. *Insets* show qualitatively normal basal infoldings (*A'* and *B'*) and microvilli and disc alignment (*A"* and *B"*). Note the disorganized outer segments in *Irbp*$^{-/-}$ and *Irbp*$^{-/-}$;*Rrh*$^{-/-}$ tissues. Images are representative of at least 10 images from two mice. *Scale bars*, 1 μm.

trans-ROL transit as loss of peropsin or IRBP alone. These observations suggest that peropsin and IRBP may act at similar points in the retinoid transport pathway.

Unlike *Rrh*$^{-/-}$, *Irbp*$^{-/-}$ mice also exhibit photoreceptor degeneration (Fig. 3*C*). The rate of photoreceptor degeneration in *Irbp*$^{-/-}$;*Rrh*$^{-/-}$ (*p* < 0.001) mice was similar to the rate in *Irbp*$^{-/-}$ mice (*p* < 0.001) (Fig. 3, *C–E*), and the RPE/OS ultrastructure was similarly disorganized (Fig. 4, *C* and *D*). Partial degeneration of photoreceptors is responsible for the lower levels of 11-*cis*-RAL in dark-adapted *Irbp*$^{-/-}$ and *Irbp*$^{-/-}$;*Rrh*$^{-/-}$ *versus* wild-type retinas (Fig. 5*A*).

Levels of visual-cycle proteins in retinas and RPE from wild-type and Rrh$^{-/-}$ mice

After uptake into the RPE cell, all-*trans*-ROL binds to CRBP1 (29). All-*trans*-ROL bound to CRBP1 is the preferred substrate for lecithin–retinol acyltransferase (LRAT), which esterifies retinol with a fatty acid from phosphatidylcholine (30, 31). Rpe65, the retinoid isomerase in RPE cells, uses all-*trans*-REs, such as all-*trans*-retinyl palmitate, as substrate to synthesize 11-*cis*-ROL (32–34). Changes in the levels of CRBP1, LRAT, or Rpe65 could affect all-*trans*-RE levels in *Rrh*$^{-/-}$ mice. Accordingly, we measured levels of these proteins in RPE homogenates from dark- or light-adapted wild-type and *Rrh*$^{-/-}$ mice by immunoblotting. We observed no significant difference in the
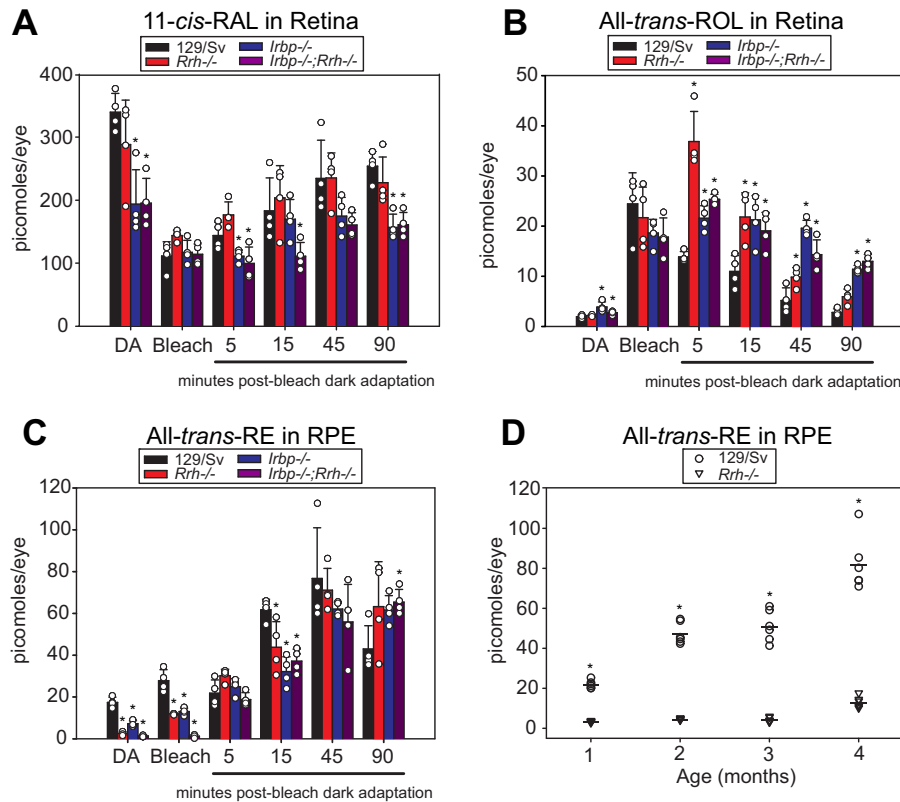
Figure 5. Retinoid dynamics in 129/Sv, $Rrh^{-/-}$, $Irbp^{-/-}$, and $Irbp^{-/-};Rrh^{-/-}$ mice. Overnight dark-adapted mice of each genotype were exposed to white light at 1,000 lux for 5 min and allowed to recover in the dark for 5, 15, 45, or 90 min. Eyes were dissected, RPE and neural retina were separated, and retinoids were analyzed by HPLC. *A*, 11-*cis*-RAL levels in the retina. The levels of 11-*cis*-RAL in retinas from 129/Sv and $Rrh^{-/-}$ mice were not statistically different ($p = 0.181$), whereas $Irbp^{-/-}$ and $Irbp^{-/-};Rrh^{-/-}$ mice tended to have lower levels overall due to photoreceptor degeneration ($p < 0.001$) and were significantly different than 129/Sv per time point as denoted by * ($p < 0.050$). *B*, all-*trans*-ROL levels in the retina. Note that all-*trans*-ROL increases after the photobleach and steadily decreases during postbleach recovery in 129/Sv mice, whereas all-*trans*-ROL remains elevated through 90-min postbleach recovery in $Rrh^{-/-}$ ($p < 0.001$), $Irbp^{-/-}$ ($p < 0.001$), and $Irbp^{-/-};Rrh^{-/-}$ ($p < 0.001$) retinas. *C*, all-*trans*-RE levels in the RPE. Note the lower all-*trans*-RE during dark adaptation and immediately after photobleach in $Rrh^{-/-}$ ($p < 0.009$), $Irbp^{-/-}$ ($p < 0.019$), and $Irbp^{-/-};Rrh^{-/-}$ ($p < 0.002$) *versus* 129/Sv RPE. Also note that all-*trans*-RE levels increase in the three mutant mice during postbleach recovery, eventually catching up and overtaking levels in the wild-type RPE. In *A*–*C*, *DA* represents dark-adapted. Data are plotted as measurements from a single eye (○) overlaid with mean ± S.D. (*error bars*) of $n = 4$ mice. Significant differences ($p < 0.050$) in time points as compared with 129/Sv are denoted by *. *D*, age-dependent accumulation of all-*trans*-RE in the eyes of dark-adapted 129/Sv and $Rrh^{-/-}$ mice. Note the 4-fold increase in dark-adapted all-*trans*-RE levels in wild-type mice between 1 and 4 months, whereas all-*trans*-RE levels remain relatively unchanged in $Rrh^{-/-}$ mice. Data are plotted as measurements from a single eye from $n = 6$ mice with the mean indicated by a *horizontal black bar*. Significant differences between 129/Sv (○) and $Rrh^{-/-}$ (▽) at each age ($p < 0.050$) are denoted by *.

levels of CRBP1, LRAT, or Rpe65 in wild-type or $Rrh^{-/-}$ RPE homogenates (p values >0.119) from dark- or light-adapted mice (p values >0.060) (Fig. 6). These data exclude the possibility that loss of peropsin affects the levels of other RPE proteins involved in the synthesis or depletion (or mobilization) of retinyl esters. These data also exclude the possibility that peropsin modulates expression of these proteins in a light-dependent fashion.

Vitamin A uptake and processing by RPE eyecup explants

To determine whether peropsin affects the rate of all-*trans*-ROL esterification in RPE cells, we measured *de novo* synthesis of all-*trans*-RE from exogenous all-*trans*-[³H]ROL by dark- and light-adapted wild-type and $Rrh^{-/-}$ mouse eyecups. Although levels of endogenous retinyl esters differed markedly between wild-type and $Rrh^{-/-}$ eyecups ($p < 0.001$), we observed no differences in newly synthesized all-*trans*-[³H]RE between dark- or light-adapted wild-type or $Rrh^{-/-}$ eyecups ($p = 0.900$) (Fig. 7). These data suggest that the lower retinyl esters in $Rrh^{-/-}$ *versus* wild-type RPE are not caused by reduced retinyl ester synthesis.

Vitamin A processing in RPE homogenates

To measure retinyl ester synthesis and hydrolysis rates directly, we prepared protein homogenates from dark- and light-adapted eyecups from $Rrh^{-/-}$ or 129/Sv mice. For retinyl ester synthesis, we added all-*trans*-ROL substrate to the homogenates and measured the amount of retinyl ester formed by HPLC (Fig. 8A). We observed no difference in the rates of ester formation in eyecup homogenates from mice of either genotype ($p = 0.295$). We also observed no difference in the rates of ester synthesis by homogenates from dark- or light-adapted mice (p values >0.055). These results are in agreement with those from the explant experiments, providing further evidence that retinyl ester synthase activity in RPE cells is not affected by loss of peropsin.

A third possible explanation for the low retinyl esters in the RPE of dark-adapted $Rrh^{-/-}$ mice is increased retinyl ester hydrolase activity. The protein responsible for simple hydrolysis of all-*trans*-REs in the RPE has not yet been identified. To assay for this activity, we prepared RPE-containing eyecup homogenates from dark- or light-adapted wild-type and
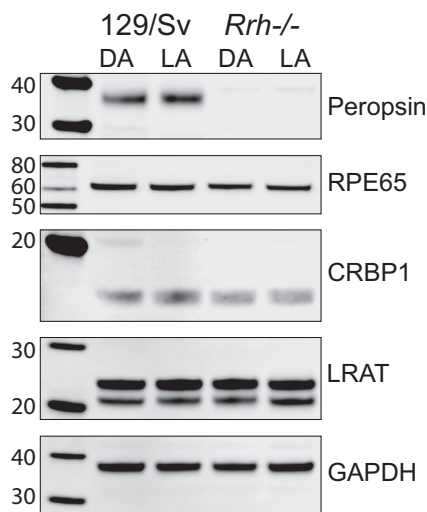
Figure 6. Immunoblots showing the abundance of retinoid-processing proteins in 129/Sv and *Rrh*$^{-/-}$ RPE. RPE homogenates were prepared from 1-month-old overnight dark-adapted mice and mice additionally exposed to 2 h of 1,000-lux white light. Samples were probed using antibodies against peropsin, Rpe65, CRBP1, LRAT, and GAPDH. Note that Rpe65 ($p = 0.119$), CRBP1 ($p = 0.193$), and LRAT ($p = 0.792$) levels are not significantly affected by light exposure or the absence of peropsin. GAPDH is used here as a loading control. Pixel density was quantified using ImageStudio software (LI-COR Biosciences) and normalized to the loading control. Images are representative of $n > 3$ independent samples.
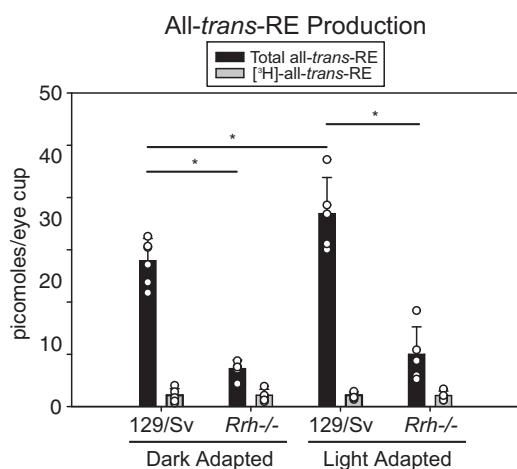

Figure 7. Retinyl ester synthesis in whole RPE eyecup explants. Mouse eyecup explants were incubated with exogenous 5 μM all-*trans*-ROL spiked with all-*trans*-[^{3}H]ROL bound to 5 μM IRBP in the dark or under 1,000-lux UV-filtered white light for 5 min. Samples were washed extensively prior to homogenization and retinoid analysis. Total (*black bars*) and newly synthesized all-*trans*-[^{3}H]REs (*gray bars*) in RPE eyecups after incubation in the dark or light are shown. Note the 5-fold lower levels of total all-*trans*-RE in *Rrh*$^{-/-}$ *versus* 129/Sv eyecups ($p < 0.001$). These levels increase slightly upon light adaptation in 129/Sv mice ($p < 0.001$). We failed to show a significant increase upon light adaptation in *Rrh*$^{-/-}$ ($p = 0.29$). Also note that *de novo* synthesized all-*trans*-[^{3}H]RE was similar in the four eyecup samples, suggesting no change in *de novo* retinyl ester synthase activity. Quantifications of single eyecups are plotted as *circles* (○) along with the mean ± S.D. (*error bars*) of $n = 5$ mice per condition. Significant differences ($p < 0.050$) are denoted by *.

Rrh$^{-/-}$ mice. These homogenates were incubated with all-*trans*-retinyl acetate (all-*trans*-RAc), a relatively soluble form of retinyl ester. We removed aliquots at different times during the incubations and quantitated remaining all-*trans*-RAc by HPLC. Approximately 90% of the all-*trans*-RAc substrate was consumed during the 30-min incubation (Fig. 8*B*). The rates of
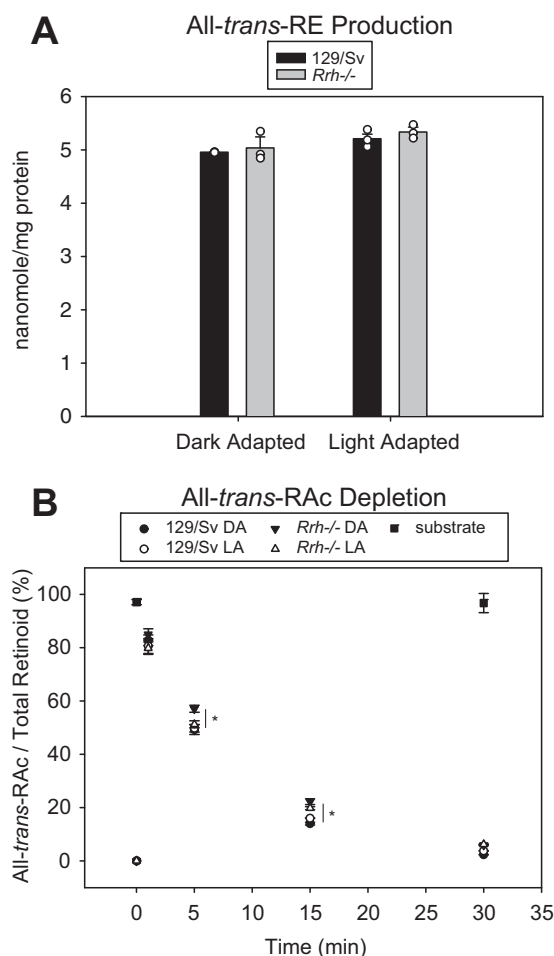

Figure 8. Synthesis and hydrolysis of retinyl esters by eyecup homogenates. Activities were measured in homogenates from 129/Sv and *Rrh*$^{-/-}$ mice after overnight dark adaptation (*DA*) or 2 h of light adaptation (*LA*). *A*, retinyl ester synthase activity. Homogenates were incubated with 2 μM all-*trans*-ROL at 37 °C for 4 min. Data are plotted as *circles* (○) along with the mean ± S.D. ($n = 3$). Note the similar amounts of all-*trans*-retinyl palmitate produced during incubation by the four eyecup homogenates, suggesting similar LRAT activities ($n = 3$, $p > 0.050$). *B*, retinyl ester hydrolysis by RPE homogenates. The hydrolysis reaction was initiated by the addition of 10 μM all-*trans*-RAc. Incubations were performed for 1, 5, 15, and 30 min, and all-*trans*-RAc content was measured by HPLC. All-*trans*-RAc substrate levels persisted throughout the assay in the absence of homogenate (■). Levels are expressed as the percentage of total all-*trans*-RAc added and have been normalized to unity over the value at $t = 0$. The data were fit with simple exponential functions, $e^{-k \cdot t}$, which were not shown for clarity, and rate constant units are min^{-1}: 129/Sv dark-adapted, 0.014 ± 0.01 (●);129/Sv light-adapted, 0.014 ± 0.02 (○); *Rrh*$^{-/-}$ dark-adapted, 0.011 ± 0.01 (▼); *Rrh*$^{-/-}$ light-adapted, 0.013 ± 0.02 (△). Data are shown as the mean ($n = 3$), and the *error bars* represent S.D. The errors for the rate constants were obtained from the curve fits.

all-*trans*-RAc depletion were similar in homogenates from the four mouse experimental conditions (Fig. 8*B*), although the data did reveal a statistically significant difference (p values <0.050): retinyl ester hydrolysis activity in *Rrh*$^{-/-}$ homogenates was actually slightly slower that the 129/Sv homogenate control. Therefore, these differences do not explain our *in vivo* observations and may not be biologically relevant. Furthermore, we observed no differences in the rates of retinyl ester hydrolysis between homogenates from dark-adapted *versus* light-exposed mice. These results suggest that peropsin plays no role in regulating retinyl ester hydrolysis.

Discussion

Peropsin is a non-visual opsin of ancient origin in both vertebrates and invertebrates. In the vertebrate eye, it is expressed in the apical microvilli of RPE cells facing the OS of photoreceptors across the interphotoreceptor matrix (IPM). Unlike the visual opsins in rods and cones, invertebrate peropsin homologues bind all-*trans*-RAL in the dark and isomerize it to 11-*cis*-RAL upon exposure to light (18, 19). This "reverse" photoisomerase activity of peropsin is similar to that of RGR opsin (10) and squid retinochrome (35), which are thought to synthesize 11-*cis*-RAL chromophore for regeneration of visual opsins. Peropsin is unlikely to serve this function, however, because wild-type and $Rrh^{-/-}$ retinas contained similar levels of 11-*cis*-RAL following a photobleach (Fig. 5A). Based on sequence homology, peropsin is likely a bistable pigment whereby the chromophore remains covalently coupled to the opsin after photoisomerization (36). Peropsin includes the conserved (E/D)R(Y/W/F) and NP$XXYX_{5,6}$F motifs, which are critical for the interaction of a G protein–coupled receptor with its G protein (37, 38). These observations suggest that peropsin is a light-signaling molecule in the RPE. A recent report suggests vertebrate peropsin may also act as a light sensor in skin keratinocytes (25). The normal retinal anatomy observed in $Rrh^{-/-}$ mice (Figs. 3 and 4) indicates that peropsin is not required for photoreceptor viability or the maintenance of RPE ultrastructure. Rods and cones diurnally shed their distal OS, which are phagocytosed by cells of the RPE (23). Animals with impaired OS phagocytosis, such as the $Mertk^{-/-}$ mouse (39), exhibit whorl-like debris in the subretinal space between the OS and RPE cells and rapid photoreceptor degeneration (39). Neither of these morphologic features were present in $Rrh^{-/-}$ mice, suggesting no essential or non-redundant role for peropsin in OS phagocytosis.

Because chromophore consumption by photoreceptors is coupled to light intensity, RPE cells may use photometric information from peropsin to regulate visual retinoid metabolism. To explore this possibility, we determined visual retinoids in retinas and RPE from normal and $Rrh^{-/-}$ mice overnight dark-adapted and at different times after a bright light. These studies revealed two persistent changes with loss of peropsin: (i) levels of all-*trans*-ROL were 2-fold higher in $Rrh^{-/-}$ *versus* wild-type retinas after the photobleach (Fig. 5B), and (ii) retinyl esters were 5-fold lower in dark-adapted $Rrh^{-/-}$ *versus* wild-type RPE (Fig. 5C). Following light exposure, photoreceptors release all-*trans*-ROL into the IPM where it binds IRBP (40) and transits the short distance to the RPE. On the apical surface of the RPE, which does not contain the Stra6 receptor for retinol-binding protein (41), the mechanism of all-*trans*-ROL uptake from the IPM is not clear. It may involve a docking or receptor-mediated interaction with another protein on the villous membrane surface. The greater affinity of all-*trans*-ROL to CRBP1 inside the cell drives uptake of all-*trans*-ROL (1), which is rapidly fatty-acylated by LRAT to form a retinyl ester. The high activity and low K_m of LRAT toward its all-*trans*-ROL substrate (42) means that all-*trans*-REs are an indicator of all-*trans*-ROL, which is usually present at low concentrations in RPE cells. Mice lacking IRBP (26) or CRBP1 (43) exhibit elevated all-*trans*-ROL in the retina and reduced all-*trans*-REs in the RPE due to impaired transit of all-*trans*-ROL from photoreceptor OS to RPE. The similar retinoid phenotypes in $Rrh^{-/-}$, $Irbp^{-/-}$, and $Crbp1^{-/-}$ mice supports the hypothesis that peropsin plays a role in the movement of all-*trans*-ROL from photoreceptors to the RPE.

We sought to identify the cause of low retinyl esters in the RPE of $Rrh^{-/-}$ mice. Three proteins directly affect all-*trans*-RE levels in the RPE: CRBP1, LRAT, and Rpe65. These proteins were present at similar abundances under the four conditions of light exposure and genotype (Fig. 6), ruling out the possibility that light exposure or loss of peropsin affects CRBP1, LRAT, or Rpe65 abundance. The rates of all-*trans*-RE synthesis by RPE-containing eyecups were also similar under these four conditions (Fig. 7). Enzyme assays on RPE homogenates from wild-type and $Rrh^{-/-}$ mice in light- or dark-adapted states also showed no difference in LRAT catalytic activity (Fig. 8A). Finally, we found that the rates of retinyl acetate hydrolysis in RPE homogenates from dark- or light-adapted wild-type and $Rrh^{-/-}$ mice were similar (Fig. 8B). Together, these findings suggest that the lower retinyl esters in $Rrh^{-/-}$ RPE are probably not caused by changes in retinyl ester synthase or hydrolase activities of the visual cycle but may reflect regulation by peropsin of all-*trans*-ROL uptake into the RPE.

Several possible mechanisms that explain peropsin modulation of all-*trans*-ROL uptake into RPE cells are consistent with the results presented here. (*a*) Peropsin may serve as the receptor or docking site for holo-IRBP on the RPE apical microvillus membrane. This would place IRBP in position to transfer its all-*trans*-ROL cargo to CRBP1 inside the cell. The affinity of IRBP binding to peropsin may be regulated by ambient light. (*b*) Peropsin may modulate the affinity of the IRBP receptor on the apical RPE surface for its IRBP ligand in a light-dependent fashion. The IRBP receptor has not been identified. (*c*) Peropsin may modulate by light the affinity of CRBP1 inside the cell to the IRBP receptor, to phospholipid headgroups on the inner villous membrane, or to cytoskeletal proteins associated with the inner villous membrane. Any of these actions would inhibit transfer of all-*trans*-ROL from IRBP to CRBP1 and hence uptake of all-*trans*-ROL into the RPE cell. (*d*) Finally, peropsin may modulate the affinity of CRBP1 for its all-*trans*-ROL ligand or the affinity of holo-CRBP1 to LRAT for esterification of all-*trans*-ROL.

How does regulating uptake of all-*trans*-ROL into RPE cells benefit the visual system? Given the low K_m of LRAT for all-*trans*-ROL (42) and the low turnover rate of Rpe65 (32, 44), the RPE visual cycle supplies chromophore to rods in dim light with low fluxes of all-*trans*-ROL. In contrast, the retinoid isomerase in Müller cells, DES1, has a much higher turnover rate than does Rpe65 (3, 4). Furthermore, Müller cells release the chromophore precursor, 11-*cis*-ROL, into the IPM (3, 45). Because only cones can utilize 11-*cis*-ROL to regenerate visual pigments (44, 46), the Müller cell visual cycle is optimized to provide cones with chromophore precursor under bright light conditions. In dim light, peropsin may accelerate uptake of all-*trans*-ROL into RPE cells, diverting all-*trans*-ROL from the Müller cell pathway. In the absence of peropsin, all-*trans*-ROL uptake by RPE cells is reduced, explaining the lower all-*trans*-RE levels in dark-adapted $Rrh^{-/-}$ mice (Fig. 5C). In bright light, peropsin may limit uptake of all-*trans*-ROL into the RPE, diverting it to Müller cells. Thus, peropsin may serve as a diverter valve, send-

ing all-*trans*-ROL to the RPE or Müller cell visual cycle depending on light conditions.

Experimental procedures

Animal use and care statement

This study was carried out in accordance with recommendations in the Guide for the Care and Use of Laboratory Animals of the National Institutes of Health and the Association for Research in Vision and Ophthalmology statement for the use of animals in ophthalmic and vision research. Euthanasia was performed by cervical dislocation on deeply anesthetized (10 mg/kg xylazine and 100 mg/kg ketamine) mice to minimize pain and distress.

Targeted disruption of the Rrh gene and generation of Rrh$^{-/-}$ mice

A mouse *Rrh* genomic fragment was used to construct a targeting vector (Fig. 1*A*). We replaced a 4.3-kb fragment starting at the initiator methionine in exon 1 and encompassing the 5′ 60% of intron 1 with a *LacZ*-coding region followed by a neomycin resistance cassette (*PGK-Neo*). This insert deletes the first 36 codons of the *Rrh* open reading frame (present within exon 1), removes the exon 1-intron 1 splice donor site, and introduces two transcription termination sites into the transcription unit: one at the 3′-end of the *LacZ* reporter and a second one at the 3′-end of the *PGK-Neo* cassette. Within that part of the *Rrh* open reading frame that remains in the targeted allele (starting in exon 2), the next in-frame ATG codon (*i.e.* potential initiator methionine codon) is at codon 81 between the second and third predicted transmembrane segments. If transcription proceeded through the remaining *Rrh* exons and the resulting mRNA were to be translated, the translation product would include only five of the seven predicted transmembrane segments. Thus, the knock-out allele is very likely to completely eliminate *Rrh* function. The 5′ homology arm extends from the initiator methionine codon in exon 1 to an EcoRI site 6.7 kb 5′ of that location; the 3′ homology arm extends 2.6 kb from a HindIII site in intron 1, 60% of the distance from exon 1, to the 3′-end of exon 2. The thymidine kinase gene was inserted in the vector adjacent to the 3′ homology arm to counterselect against non-homologous recombinants with ganciclovir treatment. The targeting vector was linearized at the 5′ edge of the 5′ homology arm and electroporated into ES cells. After selection, the G418- and ganciclovir-resistant clones were screened by Southern blotting and introduced into blastocysts. The progeny of the resulting chimeric mice were screened by Southern blotting (Fig. 1*B*). Genomic DNA was digested with KpnI and probed with a fragment from *Rrh* exon 2 and a fragment from *LacZ*. Tail DNA was analyzed by PCR to detect the presence of the *Neo* cassette (5′-GGCCA-CAGTCGATGAATCCAGAA-3′ and 5′-TGATGCCGCCGT-GTTCCGGCTGT-3′) or the *Rrh* wild-type allele (5′-TGAAC-TTACACACCAGATCTGCAG-3′ and 5′-CTGAGTGA-GGCTTCGGATTTTAAC-3′). Homozygous mutants were crossed with 129/Sv mice for at least eight generations and confirmed to be on a background containing the normal *Rpe65* Leu/Leu-450 and wild-type *Rd8* alleles. It should be noted that for all studies comparisons were made using 129/Sv and *Rrh*$^{-/-}$ of a semimixed background.

Antibodies and immunoblotting

A custom immunogen affinity-purified antibody was made in rabbits by immunizing with a peptide corresponding to the carboxyl-terminal 41 residues of mouse peropsin (CHKKFRK-AMLAMFKAQPHLAVPEPSTLPMDMPQSSLAPVRI) conjugated to keyhole limpet hemocyanin (YenZym, San Francisco, CA). Anti-Rpe65 antiserum was prepared as described previously (47). Anti-LRAT antiserum was a gift from Palczewski and co-workers (48). Protein extracts from dissected eyecups were homogenized in phosphate-buffered saline (PBS) + 0.05% *n*-dodecyl β-D-maltoside containing protease inhibitor, incubated with Benzonase nuclease (Invitrogen) overnight at 4 °C, and clarified by microcentrifugation. SDS-polyacrylamide gels were run with 20 µg of protein/lane, transferred to PVDF membrane (Millipore), and blocked with Odyssey Blocking Buffer (LI-COR Biosciences) for 1 h. Membranes were incubated with primary antibody (1:1,000) overnight at 4 °C followed by three washes in PBS + 0.1% Tween 20 (PBST). Secondary antibodies (donkey anti-mouse IRDye 680 or donkey anti-rabbit IRDye 800, LI-COR Biosciences) were applied for 1 h at 1:10,000 dilutions followed by three washes in PBST and imaged using a LI-COR Biosciences Odyssey CLx infrared imaging system.

Immunohistochemistry

After euthanizing the mice, a corneal window was cut into whole enucleated eyes and fixed for 30 min at room temperature or overnight at 4 °C in 4% paraformaldehyde diluted in PBS. Eyecups were marked for orientation, and the anterior section and lens were removed. Tissues were cryopreserved first in 10% and then 30% sucrose solutions in PBS before embedding in OCT (TissueTek) and cut into 10-µm sections. Sections were prepared as described previously (4). Primary (YenZym) and secondary (Alexa Fluor 488 donkey anti-rabbit) antibodies were used at 1:100 dilutions. Images were collected using an Olympus FluoView FV1000 confocal laser-scanning microscope equipped with 40× and 60× oil immersion objectives. Images were minimally processed using Fiji software (49).

Light and electron microscopy

Mice under deep anesthesia with isoflurane were fixed by intracardiac perfusion with 2% formaldehyde and 2.5% glutaraldehyde in 0.1 M sodium phosphate buffer, pH 7.2. Light cautery was applied at the superior pole of the cornea to mark the orientation before enucleation of the eyeball. The eyecup was trimmed into temporal and nasal hemispheres. All tissues were immersed for 1 h in 1% osmium tetroxide dissolved in 0.1 M sodium phosphate buffer (pH 7.4) followed by dehydration in a graded series of alcohols. The temporal hemispheres were embedded in an Epon/Araldite mixture. Light microscope sections were cut at 1 µm, stained with 1% toluidine blue and 1% sodium borate, and then photographed with a Zeiss Axiophot microscope fitted with a Planapo 20× lens and a CoolSNAP digital camera. The nasal hemispheres were cut in quadrants and embedded in Araldite 502 (Ted Pella, Redding, CA) for electron microscopy. Ultrathin sections for electron microscopy were cut on a Leica Ultracut ultramicrotome. The sections were collected on 200-mesh copper grids and stained with uranium and lead salts before viewing on a Zeiss 910 electron microscope. Electron

microscopic images were acquired from the superior nasal quadrant sections using a KeenView™ digital camera.

Retinoid dynamics assay

Overnight dark-adapted mice were anesthetized using a mixture of xylazine and ketamine at 10 mg/kg and 100 mg/kg, respectively, and pupils were dilated using eye drops containing 2.5% phenylephrine HCl solution. Mice were bleached with 1,000-lux white light for 5 min in a Ganzfield dome and returned to dark for 0, 5, 15, 45, and 90 min before sacrifice, enucleation, and dissection of RPE eyecup and retina. Equal numbers of male and female mice were analyzed at 4–6 weeks of age. Measurements represent analysis from a single eye from four mice for each time point. Tissues were homogenized using a glass–glass homogenizer in 500 μl of PBS + 200 mM hydroxylamine + protease inhibitor and analyzed for retinoids by HPLC as described previously (12).

All-trans-[³H]retinol uptake in mouse eyecups

Eyecups were prepared from 129/Sv and $Rrh^{-/-}$ overnight dark-adapted mice. Eyes were enucleated, and the anterior section and lens were removed. The retina was separated, and the eyecup containing RPE was washed in PBS at room temperature. The eyecups were then submerged in a solution containing 5 μM holo-IRBP with 1 eq of all-trans-[³H]retinol (~10,000 dpm/pmol) in DMEM for 30 min at 37 °C followed by three washes in PBS. Eyecups were homogenized using a glass–glass homogenizer in a total volume of 500 μl of PBS and extracted twice in cold hexane/methanol (1.5 ml each). The non-polar phase containing the retinoid was dried, resuspended in 100 μl of hexane, and analyzed by HPLC equipped with a Packard 500TR flow scintillation counter calibrated for tritium.

LRAT assay

RPE eyecups were collected from overnight dark-adapted mice or mice additionally exposed to 1,000-lux UV-filtered white light for 2 h. All subsequent procedures were performed under dim red light. Homogenates were prepared in PBS + protease inhibitor, and cells were disrupted using a glass–glass homogenizer. Samples contained 10 μg of protein homogenate in 10 mM Tris (pH 8.0), 2 mM CaCl$_2$, 2 mM MgCl$_2$, 1 mM DTT, and 1% BSA. After 2 min of preincubation in a 37 °C water bath, the reaction was initiated with the addition of 2 μM all-trans-retinol delivered in DMSO in the dark. The reaction was quenched after 4 min with cold methanol and extracted with hexane for retinoid analysis.

Retinyl ester hydrolase assay

RPE homogenates were prepared as above. Samples contained 10 μg of protein homogenate in 50 mM Tris (pH 8.0) with 1% BSA. After 2 min of preincubation in a 37 °C water bath, the reaction was initiated with the addition of 10 μM all-trans-RAc delivered in ethanol in the dark. Aliquots were removed at 0, 1, 5, 15, and 30 min from the bulk reaction mixture and quenched with cold methanol, and the retinoids were extracted in hexane.

Statistical analysis

Data were analyzed in the Statistical Package for Social Scientists, version 24 (SPSS; IBM), using separate but parallel analyses of variance (linear mixed models) with the relevant measure (retinal thickness, 11-cis-RAL, all-trans-ROL, all-trans-RE, all-trans-RAc, or pixel density) as the dependent variable and genotype, time, and light status as independent variables as necessary. Post hoc tests were performed only when the initial omnibus tests showed significance. Statistical significance was defined as $p < 0.050$.

Author contributions—H. S. and J. N. conceived, designed, and created the knock-out mouse. J. D. C. carried out all studies analyzing the knock-out mouse solely or in collaboration with S. Y. N. (morphology, protein expression, and enzyme assays), R. A. R. (retinoid dynamics), M. L. (EM studies), and D. B. (EM studies). S. E. prepared microscopy sections. J. D. C. analyzed the data with assistance from D. B. (EM studies) and R. A. R. (retinoid dynamics). J. D. C., R. A. R., and G. H. T. conceived the study. J. D. C., R. A. R., and G. H. T. interpreted the results. J. D. C. and G. H. T. wrote the paper.

References

1. Wright, C. B., Redmond, T. M., and Nickerson, J. M. (2015) A history of the classical visual cycle. *Prog. Mol. Biol. Transl. Sci.* **134,** 433–448
2. Wang, J. S., and Kefalov, V. J. (2011) The cone-specific visual cycle. *Prog. Retin. Eye Res.* **30,** 115–128
3. Kaylor, J. J., Yuan, Q., Cook, J., Sarfare, S., Makshanoff, J., Miu, A., Kim, A., Kim, P., Habib, S., Roybal, C. N., Xu, T., Nusinowitz, S., and Travis, G. H. (2013) Identification of DES1 as a vitamin A isomerase in Müller glial cells of the retina. *Nat. Chem. Biol.* **9,** 30–36
4. Kaylor, J. J., Cook, J. D., Makshanoff, J., Bischoff, N., Yong, J., and Travis, G. H. (2014) Identification of the 11-cis-specific retinyl-ester synthase in retinal Müller cells as multifunctional O-acyltransferase (MFAT). *Proc. Natl. Acad. Sci. U.S.A.* **111,** 7302–7307
5. Kaylor, J. J., Xu, T., Ingram, N. T., Tsan, A., Hakobyan, H., Fain, G. L., and Travis, G. H. (2017) Blue light regenerates functional visual pigments in mammals through a retinyl-phospholipid intermediate. *Nat. Commun.* **8,** 16
6. Panda, S., Sato, T. K., Castrucci, A. M., Rollag, M. D., DeGrip, W. J., Hogenesch, J. B., Provencio, I., and Kay, S. A. (2002) Melanopsin (Opn4) requirement for normal light-induced circadian phase shifting. *Science* **298,** 2213–2216
7. Ruby, N. F., Brennan, T. J., Xie, X., Cao, V., Franken, P., Heller, H. C., and O'Hara, B. F. (2002) Role of melanopsin in circadian responses to light. *Science* **298,** 2211–2213
8. Lucas, R. J., Hattar, S., Takao, M., Berson, D. M., Foster, R. G., and Yau, K. W. (2003) Diminished pupillary light reflex at high irradiances in melanopsin-knockout mice. *Science* **299,** 245–247
9. Pandey, S., Blanks, J. C., Spee, C., Jiang, M., and Fong, H. K. (1994) Cytoplasmic retinal localization of an evolutionary homolog of the visual pigments. *Exp. Eye Res.* **58,** 605–613
10. Chen, P., Hao, W., Rife, L., Wang, X. P., Shen, D., Chen, J., Ogden, T., Van Boemel, G. B., Wu, L., Yang, M., and Fong, H. K. (2001) A photic visual cycle of rhodopsin regeneration is dependent on Rgr. *Nat. Genet.* **28,** 256–260
11. Pepe, I. M., and Cugnoli, C. (1992) Retinal photoisomerase: role in invertebrate visual cells. *J. Photochem. Photobiol. B* **13,** 5–17
12. Radu, R. A., Hu, J., Peng, J., Bok, D., Mata, N. L., and Travis, G. H. (2008) Retinal pigment epithelium-retinal G protein receptor-opsin mediates

light-dependent translocation of all-*trans*-retinyl esters for synthesis of visual chromophore in retinal pigment epithelial cells. *J. Biol. Chem.* **283,** 19730–19738

13. Nieto, P. S., Valdez, D. J., Acosta-Rodríguez, V. A., and Guido, M. E. (2011) Expression of novel opsins and intrinsic light responses in the mammalian retinal ganglion cell line RGC-5. Presence of OPN5 in the rat retina. *PLoS One* **6,** e26417

14. Kojima, D., Mori, S., Torii, M., Wada, A., Morishita, R., and Fukada, Y. (2011) UV-sensitive photoreceptor protein OPN5 in humans and mice. *PLoS One* **6,** e26388

15. Kang, S. W., and Kuenzel, W. J. (2015) Deep-brain photoreceptors (DBPs) involved in the photoperiodic gonadal response in an avian species, *Gallus gallus. Gen. Comp. Endocrinol.* **211,** 106–113

16. Van Gelder, R. N., and Buhr, E. D. (2016) Ocular photoreception for circadian rhythm entrainment in mammals. *Annu. Rev. Vis. Sci.* **2,** 153–169

17. Sun, H., Gilbert, D. J., Copeland, N. G., Jenkins, N. A., and Nathans, J. (1997) Peropsin, a novel visual pigment-like protein located in the apical microvilli of the retinal pigment epithelium. *Proc. Natl. Acad. Sci. U.S.A.* **94,** 9893–9898

18. Nagata, T., Koyanagi, M., Tsukamoto, H., and Terakita, A. (2010) Identification and characterization of a protostome homologue of peropsin from a jumping spider. *J. Comp. Physiol. A Neuroethol. Sens. Neural Behav. Physiol.* **196,** 51–59

19. Koyanagi, M., Terakita, A., Kubokawa, K., and Shichida, Y. (2002) Amphioxus homologs of Go-coupled rhodopsin and peropsin having 11-cis- and all-trans-retinals as their chromophores. *FEBS Lett.* **531,** 525–528

20. Hao, W., Chen, P., and Fong, H. K. (2000) Analysis of chromophore of RGR: retinal G-protein-coupled receptor from pigment epithelium. *Methods Enzymol.* **316,** 413–422

21. Montell, C. (2012) *Drosophila* visual transduction. *Trends Neurosci.* **35,** 356–363

22. Strauss, O. (2005) The retinal pigment epithelium in visual function. *Physiol. Rev.* **85,** 845–881

23. Young, R. W., and Bok, D. (1969) Participation of the retinal pigment epithelium in the rod outer segment renewal process. *J. Cell Biol.* **42,** 392–403

24. LaVail, M. M. (1976) Rod outer segment disk shedding in rat retina: relationship to cyclic lighting. *Science* **194,** 1071–1074

25. Toh, P. P., Bigliardi-Qi, M., Yap, A. M., Sriram, G., and Bigliardi, P. (2016) Expression of peropsin in human skin is related to phototransduction of violet light in keratinocytes. *Exp. Dermatol.* **25,** 1002–1005

26. Jin, M., Li, S., Nusinowitz, S., Lloyd, M., Hu, J., Radu, R. A., Bok, D., and Travis, G. H. (2009) The role of interphotoreceptor retinoid-binding protein on the translocation of visual retinoids and function of cone photoreceptors. *J. Neurosci.* **29,** 1486–1495

27. Katz, M. L., Drea, C. M., and Robison, W. G., Jr. (1987) Dietary vitamins A and E influence retinyl ester composition and content of the retinal pigment epithelium. *Biochim. Biophys. Acta* **924,** 432–441

28. Liou, G. I., Fei, Y., Peachey, N. S., Matragoon, S., Wei, S., Blaner, W. S., Wang, Y., Liu, C., Gottesman, M. E., and Ripps, H. (1998) Early onset photoreceptor abnormalities induced by targeted disruption of the interphotoreceptor retinoid-binding protein gene. *J. Neurosci.* **18,** 4511–4520

29. Huang, J., Possin, D. E., and Saari, J. C. (2009) Localizations of visual cycle components in retinal pigment epithelium. *Mol. Vis.* **15,** 223–234

30. Saari, J. C., and Bredberg, D. L. (1989) Lecithin:retinol acyltransferase in retinal pigment epithelial microsomes. *J. Biol. Chem.* **264,** 8636–8640

31. MacDonald, P. N., and Ong, D. E. (1988) A lecithin:retinol acyltransferase activity in human and rat liver. *Biochem. Biophys. Res. Commun.* **156,** 157–163

32. Jin, M., Li, S., Moghrabi, W. N., Sun, H., and Travis, G. H. (2005) Rpe65 is the retinoid isomerase in bovine retinal pigment epithelium. *Cell* **122,** 449–459

33. Moiseyev, G., Chen, Y., Takahashi, Y., Wu, B. X., and Ma, J. X. (2005) RPE65 is the isomerohydrolase in the retinoid visual cycle. *Proc. Natl. Acad. Sci. U.S.A.* **102,** 12413–12418

34. Redmond, T. M., Yu, S., Lee, E., Bok, D., Hamasaki, D., Chen, N., Goletz, P., Ma, J. X., Crouch, R. K., and Pfeifer, K. (1998) Rpe65 is necessary for production of 11-cis-vitamin A in the retinal visual cycle. *Nat. Genet.* **20,** 344–351

35. Ozaki, K., Hara, R., Hara, T., and Kakitani, T. (1983) Squid retinochrome. Configurational changes of the retinal chromophore. *Biophys. J.* **44,** 127–137

36. Tsukamoto, H., and Terakita, A. (2010) Diversity and functional properties of bistable pigments. *Photochem. Photobiol. Sci.* **9,** 1435–1443

37. Franke, R. R., Sakmar, T. P., Graham, R. M., and Khorana, H. G. (1992) Structure and function in rhodopsin. Studies of the interaction between the rhodopsin cytoplasmic domain and transducin. *J. Biol. Chem.* **267,** 14767–14774

38. Fritze, O., Filipek, S., Kuksa, V., Palczewski, K., Hofmann, K. P., and Ernst, O. P. (2003) Role of the conserved NPxxY(x)5,6F motif in the rhodopsin ground state and during activation. *Proc. Natl. Acad. Sci. U.S.A.* **100,** 2290–2295

39. Duncan, J. L., LaVail, M. M., Yasumura, D., Matthes, M. T., Yang, H., Trautmann, N., Chappelow, A. V., Feng, W., Earp, H. S., Matsushima, G. K., and Vollrath, D. (2003) An RCS-like retinal dystrophy phenotype in mer knockout mice. *Invest. Ophthalmol. Vis. Sci.* **44,** 826–838

40. Liou, G. I., Bridges, C. D., Fong, S. L., Alvarez, R. A., and Gonzalez-Fernandez, F. (1982) Vitamin A transport between retina and pigment epithelium—an interstitial protein carrying endogenous retinol (interstitial retinol-binding protein). *Vision Res.* **22,** 1457–1467

41. Kawaguchi, R., Yu, J., Honda, J., Hu, J., Whitelegge, J., Ping, P., Wiita, P., Bok, D., and Sun, H. (2007) A membrane receptor for retinol binding protein mediates cellular uptake of vitamin A. *Science* **315,** 820–825

42. Kaschula, C. H., Jin, M. H., Desmond-Smith, N. S., and Travis, G. H. (2006) Acyl CoA:retinol acyltransferase (ARAT) activity is present in bovine retinal pigment epithelium. *Exp. Eye Res.* **82,** 111–121

43. Saari, J. C., Nawrot, M., Garwin, G. G., Kennedy, M. J., Hurley, J. B., Ghyselinck, N. B., and Chambon, P. (2002) Analysis of the visual cycle in cellular retinol-binding protein type I (CRBPI) knockout mice. *Invest. Ophthalmol. Vis. Sci.* **43,** 1730–1735

44. Mata, N. L., Radu, R. A., Clemmons, R. C., and Travis, G. H. (2002) Isomerization and oxidation of vitamin a in cone-dominant retinas. A novel pathway for visual-pigment regeneration in daylight. *Neuron* **36,** 69–80

45. Das, S. R., Bhardwaj, N., Kjeldbye, H., and Gouras, P. (1992) Müller cells of chicken retina synthesize 11-cis-retinol. *Biochem. J.* **285,** 907–913

46. Jones, G. J., Crouch, R. K., Wiggert, B., Cornwall, M. C., and Chader, G. J. (1989) Retinoid requirements for recovery of sensitivity after visual-pigment bleaching in isolated photoreceptors. *Proc. Natl. Acad. Sci. U.S.A.* **86,** 9606–9610

47. Mata, N. L., Moghrabi, W. N., Lee, J. S., Bui, T. V., Radu, R. A., Horwitz, J., and Travis, G. H. (2004) Rpe65 is a retinyl ester binding protein that presents insoluble substrate to the isomerase in retinal pigment epithelial cells. *J. Biol. Chem.* **279,** 635–643

48. Batten, M. L., Imanishi, Y., Maeda, T., Tu, D. C., Moise, A. R., Bronson, D., Possin, D., Van Gelder, R. N., Baehr, W., and Palczewski, K. (2004) Lecithin-retinol acyltransferase is essential for accumulation of all-*trans*-retinyl esters in the eye and in the liver. *J. Biol. Chem.* **279,** 10422–10432

49. Schindelin, J., Arganda-Carreras, I., Frise, E., Kaynig, V., Longair, M., Pietzsch, T., Preibisch, S., Rueden, C., Saalfeld, S., Schmid, B., Tinevez, J. Y., White, D. J., Hartenstein, V., Eliceiri, K., Tomancak, P., and *et al.* (2012) Fiji: an open-source platform for biological-image analysis. *Nat. Methods* **9,** 676–682